Cement and Concrete Research 40 (2010) 1465–1470

Contents lists available at ScienceDirect

Cement and Concrete Research

journal homepage: http://ees.elsevier.com/CEMCON/default.asp

Resistivity of cementitious materials measured in diaphragm migration cells: The effect of the experimental set-up

B. Díaz [a], L. Freire [a], X.R. Nóvoa [a,*], B. Puga [a], V. Vivier [b]

[a] ENCOMAT Group, E.T.S.E.I, Universidade de Vigo, Campus Universitario, 36310 Vigo, Spain
[b] LISE, UPR 15 du CNRS, Université Pierre et Marie Curie, 4 Place Jussieu, 75252 Paris Cedex 05, France

ARTICLE INFO

Article history:
Received 4 November 2009
Accepted 12 May 2010

Keywords:
Migration (C)
Resistivity (C)
Mortar (E)
Cement paste (E)
Concrete (E)

ABSTRACT

Experimental measurements and numerical analysis were carried out to study the effect of the cell geometry in resistivity determinations. The resistance of the diaphragm in cement paste and mortar samples was determined using impedance spectroscopy. Numerical simulations were performed using finite element method (FEM). Several surface ratios (geometrical diaphragm surface to electrolyte-diaphragm surface, S/S') were investigated. The thickness of the diaphragm, L, was also considered.
The experimental results show a significant decrease of the apparent resistivity when the ratio S/S' increases. Similar trend was observed for increasing values of the L/S' ratio. The numerical simulations can explain the experimental findings and also allow to formulate a general rule for the design of migration and diffusion experiments in porous materials.

1. Introduction

The penetration of aggressive substances through concrete is mainly produced by diffusion and thus both the diffusion coefficient and wetting are parameters of major importance in the lifetime prediction of reinforced concrete structures. Chloride ions are the most studied aggressive ions because of the ability to induce localized break down of the protective passive film.

Motion of chloride ions in concrete-type structures is very slow and hence very long test periods are required to obtain diffusion coefficients. Typical diffusion coefficient values are in the range of 10^{-11}–10^{-12} $m^2\ s^{-1}$ [1], that is 2 to 3 orders of magnitude smaller than the ones usually determined in aqueous solutions. For this reason methods where the transport of ions can be accelerated by the application of electrical potential gradients became very popular in the last two decades. These tests have been collectively called electrical migration tests [2].

The usual experimental set-up for this kind of test includes two external compartments at both sides of the cementitious sample [3–5]: the anodic compartment contains the "downstream solution", initially without chlorides, and the cathodic compartment, which contains the "upstream solution", a chloride containing solution. The set-up is schematically depicted in Fig. 1.

In that very common experimental arrangement the total cross section of the sample (S in Fig. 1) and the cross section in contact with the electrolytic solution in compartment (S' in Fig. 1) are, in general, made as equal as possible; nevertheless, to our knowledge no systematic study exists about the effect of the geometry of the cement paste sample on the resistivity values measured.

When an electric field is applied between the two sides of a cementitious sample, the conducting nature of the material is expected to influence current distribution depending on the geometry of the system, i.e. S and S' sections, and the thickness of the sample (L in Fig. 1). The problem is similar to the one leading to a stray capacitance when measuring the impedance of dielectrics [6], which was overcome by using a guard ring so that its width is, as a general rule, at least two times the thickness of the material in order to avoid fringing problems. Those problems are of much importance in conductivity measurements in ionic solids [7–9], where surface conduction cannot be neglected in certain circumstances. The problem is usually solved by guarding the lateral sides with conducting plates attached to them. When conductivity measurements are performed in liquids, the guard ring is made coplanar to the sensing plate [10].

None of the above guarding configurations are of applicability to the situation treated in the present paper where Fig. 2 schematically shows the possible current dispersion inside the sample. As direct consequence of this current dispersion, the resistance values for the analysed samples in this type of experiments will be lower than the actual resistance values.

The main aim in this work is to perform a systematic study of the effect of the cell's geometry (S, S', and L parameters defined in Fig. 1) on the measured resistivity. The resistivity of the samples has been determined using impedance spectroscopy (IS). This technique has been largely used for the study of the microstructure of cement paste [11–17]. The high frequency domain (f>10 kHz) of the impedance spectrum obtained from cement pastes contains useful information

* Corresponding author. Tel.: +34 986812213; fax: +34 986812201.
E-mail address: rnovoa@uvigo.es (X.R. Nóvoa).

0008-8846/$ – see front matter © 2010 Elsevier Ltd. All rights reserved.
doi:10.1016/j.cemconres.2010.05.004

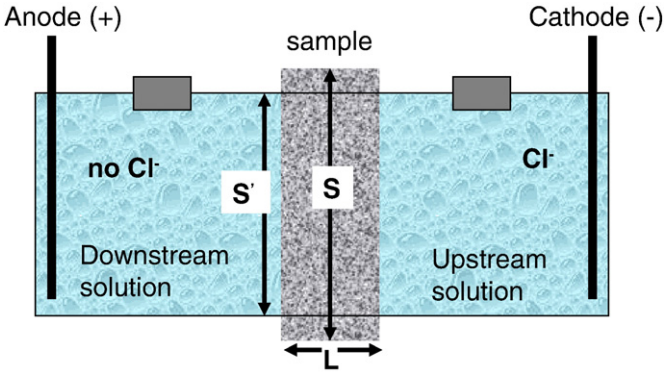

Fig. 1. Experimental set-up commonly used for electrical migration tests.

concerning several material's properties as dielectric [18,19] or mechanical [20] properties, both closely related to the porosity of the material. Moreover, IS in the high frequency domain can be employed to assess the hardening process [21,22] or chloride transport [23–25]. When cementitious samples are completely saturated, the impedance measurement is directly related to pore's connectivity, which gives good estimation of the resistivity [26].

2. Experimental

Cement paste and mortar samples were prepared using Ordinary Cement Portland CEM I 52.5R according to the composition, specifications and conformity criteria EN 197-1:2000. The water to cement ratio employed in both cases was 0.5. Samples for our experiments were cast in cylindrical moulds of 8.6 cm in diameter and 20 cm height. Slices of three different thicknesses were cut for the further experiments. For the cement paste slices of 1.2 cm, 2.6 cm and 3.7 cm thick were cut. The mortar samples were cut at 1.4 cm, 2.4 cm and 3.7 cm thick. Each sample was saturated with a 1 M NaCl solution to guarantee an adequate conductivity, following the ASTM C1202 standard [27].

Impedance measurements were performed according to the schematic diagram presented in Fig. 1. Seven different coaxial masks were employed limiting by an O-ring the contact surface between the electrolyte and the sample (S' in Fig. 1), the diameters of which were 2.6, 3.6, 4.6, 5.6, 6.6, 7.6 and 8.6 cm, respectively. Therefore, seven different ratios S/S' have been investigated ranging from 11 to 1. The impedance measurements were performed, from 40 MHz down to 100 Hz, with an HP4194A Impedance/Gain-Phase Analyser. The diameter of the capacitive response corresponds to the ionic resistance of the sample [26].

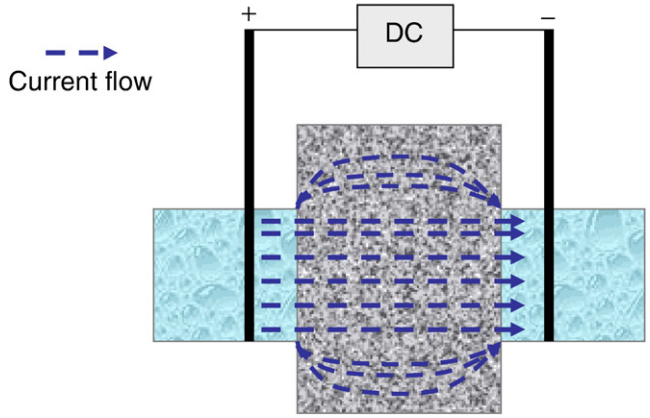

Fig. 2. Schematic current flow dispersion when applying an electric field between the two sides of a cementitious sample. $S'<S$.

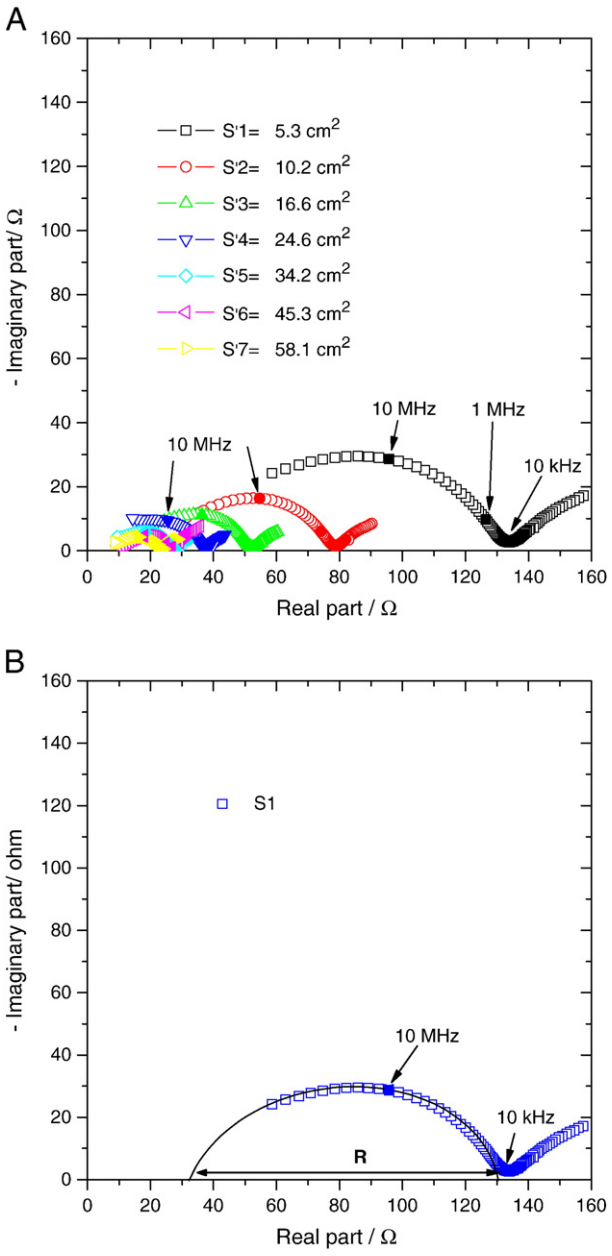

Fig. 3. (A) Impedance spectra corresponding to the 1.2 cm thick cement paste sample with the surface S' as a parameter. (B) Detail of the high frequency capacitive loop for the $S'1$ surface area, showing the determination of the resistance, R. Solid symbols denote labelled characteristic frequencies.

3-D distributions of potential and current lines were numerically computed by finite element method (FEM) using the Comsol® software with constant potentials (Dirichlet boundary conditions), +1 V and −1 V applied to the left and right hand side electrodes, respectively (Fig. 1). Simulations were performed for a wide range of geometries and conductivities. The Nernst–Planck's equation was solved through the electroneutrality condition using the GMRES solver.

3. Results and discussion

3.1. Resistivity measurements on cement paste

Fig. 3A shows the impedance spectra obtained for the thinnest cement paste analysed (1.2 cm thick) with the exposed surfaces S' as a parameter. The diameter of the high frequency arc increases as S'

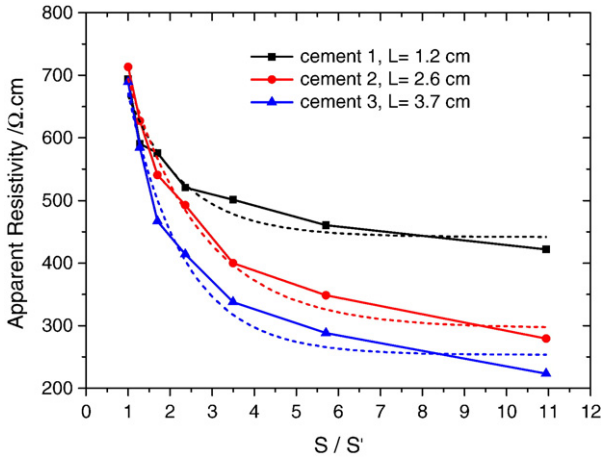

Fig. 4. Experimental apparent resistivity values (Eq. (1)) for the cement paste samples and corresponding fitting to Eq. (2) (dashed lines).

decreases. Similar tendency was observed for the thicker samples. For saturated cementitious samples resistivity can be obtained from the high frequency region (f>10 kHz), which is free from interfacial contributions [19]. When normalised with respect to sample's geometry (S' and L) the diameter of the high frequency arc allows obtaining the resistivity of the studied cementitious sample [19,28]. Therefore for each value of the surface S', the resistance value was directly gathered from the arc amplitude as described in Fig. 3B.

The apparent resistivity of the sample can then be calculated from the resistance value according to Eq. (1).

$$\rho' = R\frac{S'}{L} \tag{1}$$

Where ρ' is the apparent resistivity (Ω cm), R is the measured resistance (Ω), L is the cement paste thickness (cm) and S' is the surface of the sample (cm^2) defined by the O-ring in contact with the electrolyte.

The apparent resistivity values obtained for each of the three cement paste samples considered are plotted in Fig. 4 as a function of the S/S' ratio. Each value corresponds to an average value obtained with three different measurements. It can be seen in Fig. 4 that the resistivity obtained for the three samples converges to a single value when the S/S' ratio tends towards 1, but it decreases and diverges as the S/S' ratio increases. Such a behaviour clearly evidences that the linear dependence between R and ρ derived from Eq. (1) is not fulfilled so that the apparent resistivity is a function of the cell's geometry. Conversely, when the ratio S/S' is equal to 1, the apparent resistivity is independent of the thickness of the cementitious sample.

As it was schematically depicted in Fig. 2, when $S'<S$ the whole cement disk is also an ionic conductor so that a certain percentage of the current lines can diverge out of the cylindrical volume defined by both S' surfaces. As a result, the actual sample's volume involved in the conduction process is underestimated, and the normalization of R values considering the volume for ionic conduction "$S'\times L$" leads to

Table 1
Best fitting parameters obtained when the experimental data of Fig. 4 are modelled using Eq. (2).

L/cm	ρ_0/Ω cm	ρ_1/Ω cm	$(S/S')_1$
1.2	441.7 ± 21.6	467.0 ± 125.1	1.37 ± 0.46
2.6	295.8 ± 20.7	689.8 ± 69.1	1.82 ± 0.30
3.7	253.3 ± 22.8	885.0 ± 140.4	1.33 ± 0.26

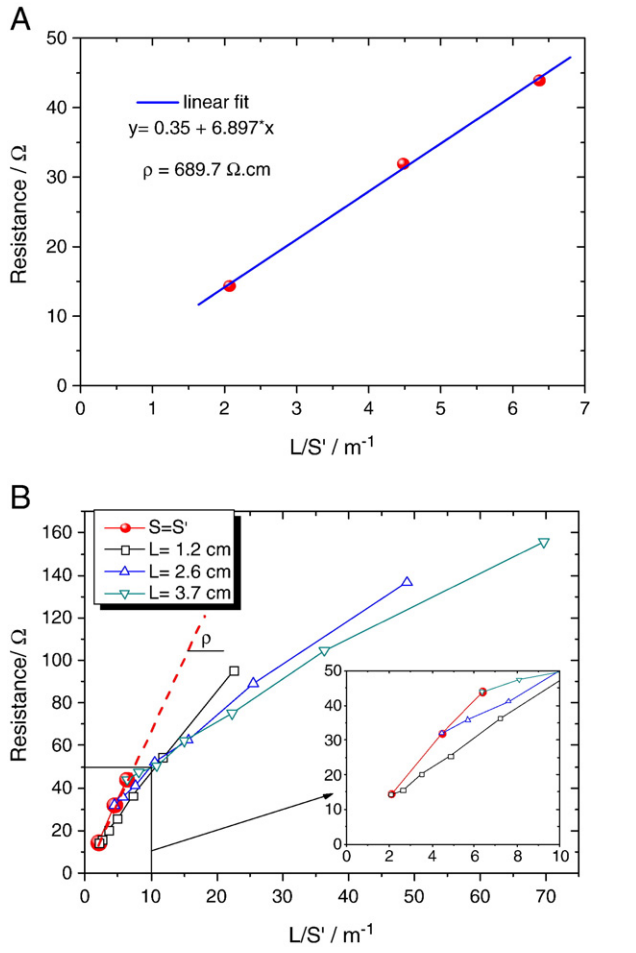

Fig. 5. (A) Resistance as a function of the L/S' parameter corresponding to $S=S'$ (thus only the thickness of the sample, L, varies). The linear fitting is also represented (dash line). (B) Resistance as a function of the L/S' parameter when $S'<S$. The case $S'=S$ is also depicted for comparison purposes.

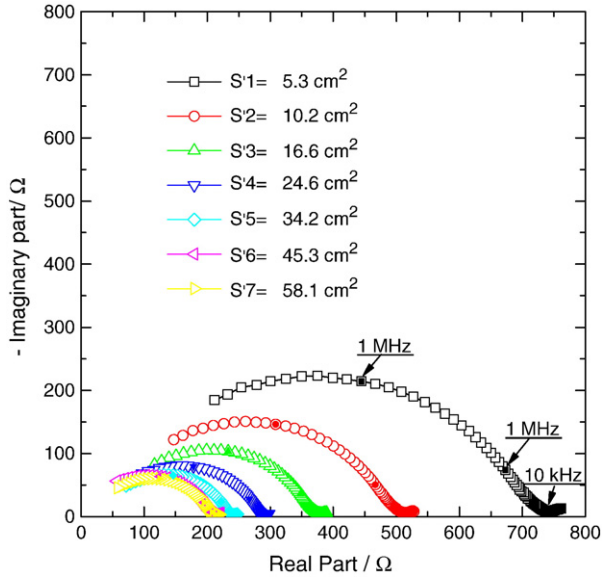

Fig. 6. Impedance spectra corresponding to a cylindrical mortar sample 2.4 cm thick, $S=58.1$ cm^2. Seven S' surfaces (mortar/electrolyte interfaces) are considered. Solid symbols denote labelled characteristic frequencies.

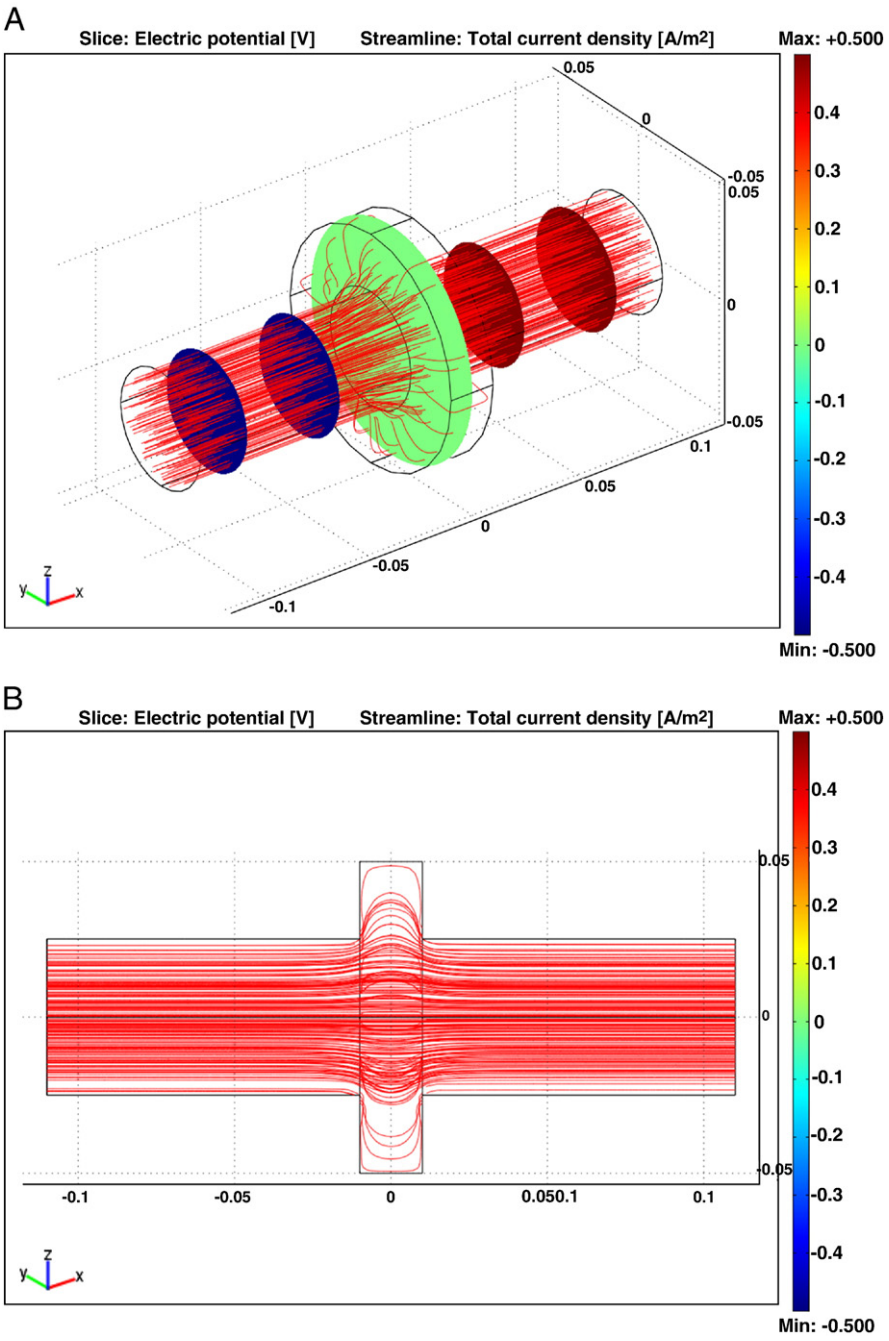

Fig. 7. Current lines obtained by FEM for a cylindrical cement paste sample ($S = 100\ cm^2$, $L = 2$ cm, and $\rho = 10^5\ \Omega cm$) entrapped between two cylinders 10 cm length and $\phi = 5$ cm ($S' = 19.6\ cm^2$) filled with electrolytic solution of conductivity 10 S m^{-1}. (A) 3D view. (B) Cross section view.

erroneous ρ estimations. Nevertheless, asymptotic type resistivity behaviour is observed for the three sets of measurements depicted in Fig. 4.

$$\rho = \rho_0 + \rho_1 \cdot e^{-x/(S/S')_1} \quad (2)$$

The experimental data were fitted to an exponential decay curve with parameters ρ_0, ρ_1 and $(S/S')_1$ (Eq. (2)) in such a way that the asymptotic values, ρ_0 in Eq. (2), can be calculated. The reason for choosing that fitting equation will be discussed later in Section 3.3. The resulting fitting, also depicted in Fig. 4 (dashed lines), gave the best fitting parameters summarised in Table 1. The smallest asymptotic apparent resistivity value corresponds to the thicker sample. Moreover, the three fitted curves converge to $\rho = 677\ \Omega$ cm for $S = S'$, within a maximum deviation of 2.5%.

If the aforementioned current dispersion in the porous material is accepted, higher deviations of the ideal "$S' \times L$" volume will correspond to geometries of small S' and large L dimensions.

3.1.1. Effect of the L/S' ratio

Another interesting issue is the dependence of the measured resistance on the L/S' ratio. According to Eq. (1), the representation of R versus L/S' should be a straight line whose slope corresponds to the sample's resistivity. Fig. 5A shows that the condition is fulfilled when $S = S'$ for the three sample's thickness investigated. However, when $S' < S$ substantial deviations from the linear behaviour occur, as shown in Fig. 5B. In the insert of Fig. 5B it can also be noted that larger deviations

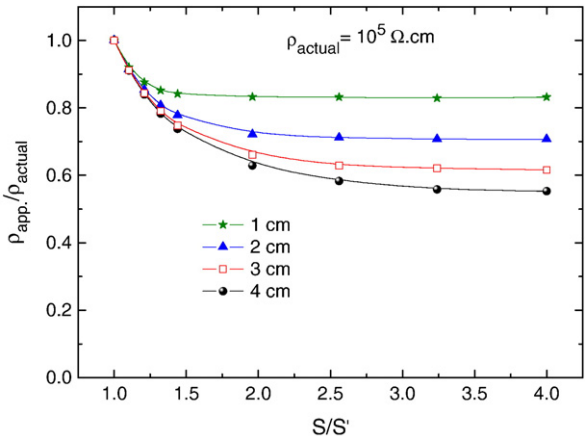

Fig. 8. Effect of the resistivity of the concrete, ρ_{actual}, on the apparent resistivity determined for the sample, $\rho_{app.}$, using Eq. (1) with the R value computed with FEM.

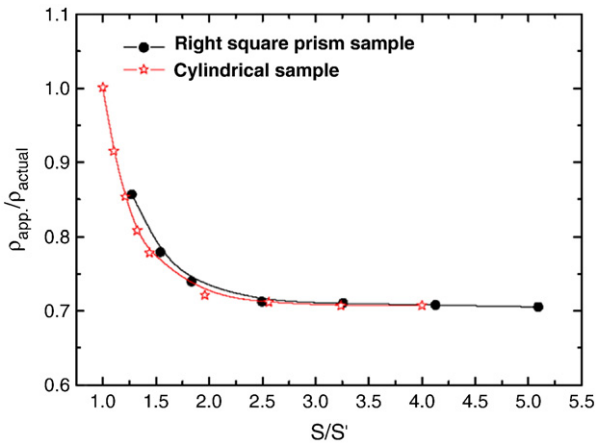

Fig. 10. Effect of the geometry and size of the sample in the apparent resistivity, $\rho_{app.}$. $\rho_{actual} = 105\ \Omega$ cm, $L = 2$ cm.

correspond to thicker samples. Deviations are always in the sense of decreasing slope, in other word, the use of $S' < S$ electrochemical-cell configuration lowers the apparent resistivity.

3.2. Resistivity measurements on mortar

Similar results were obtained for the mortar samples. In Fig. 6 the impedance plots obtained for the 2.4 cm thick sample are presented as a representative behaviour. The diameter of the capacitive arc decreases as S' increases, exhibiting the same behaviour to the one observed in Fig. 3A for cement paste samples. The only difference is the range of the resistance measured, almost one order of magnitude higher in mortar samples than in cement paste samples, as expected.

The dependences of R on S/S' and L/S' are similar to those reported in Figs. 4 and 5, respectively, thus no further comments will be incorporated here.

3.3. Numerical simulations

Distributions of potential and current in 3D space were numerically computed by FEM for cell geometries similar to those employed in the experimental measurements. Fig. 7 corresponds to the current distribution in one of the models studied. The cross section of the distribution depicted in Fig. 7A is given in Fig. 7B. As it can be seen, once current lines enter the cementitious material they tend to diverge from the initial parallel path, occupying all the volume of the sample. The situation is similar to that schematically represented in Fig. 2.

From the current and potential distributions obtained by FEM, it is possible to determine the apparent resistivity, $\rho_{app.}$, as a function of the parameters used, namely resistivity of the concrete, ρ_{actual}, and sample dimensions. $\rho_{app.}$ is obtained through Eq. (1) using the resistance value computed by FEM that accounts for fringe effects. Fig. 8 summarises the effect of the S/S' ratio as a function of the thickness of the sample. The plots showing the resistivity versus the sample's thickness summarised in Fig. 8 are similar to the experimental plots depicted in Fig. 4, which supports that the FEM calculations reproduce the experimental behaviour.

Figs. 4 and 8 show that the measured resistivity is highly dependent on L and on the S/S' ratio when this value is close to 1 (most common situations). For instance, a 9% error can be estimated for $S = 5.25$ cm and $S' = 5$ cm. However, the dependence on the conductivity of the sample and on its shape (squared shape or circular shape) is negligible, as Figs. 9 and 10 demonstrate, respectively. For instance, a variation of the resistivity of the concrete over three orders of magnitude only results in a few percent of variation in the ratio $\rho_{app.}/\rho_{actual}$ (Fig. 9), and calculations assuming a right square prism sample give the same exponential decay law than the cylindrical sample (Fig. 10).

In addition, Fig. 8 clearly shows that for $S/S' \geq 4$ a limit value for the apparent resistivity exists, $\rho_{app.}$ limit, that is a function of the

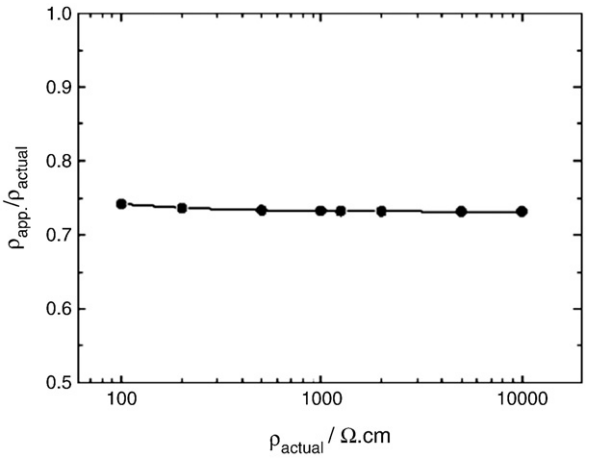

Fig. 9. Effect of the resistivity of the concrete sample, ρ_{actual}, on the apparent resistivity determined, $\rho_{app.}$.

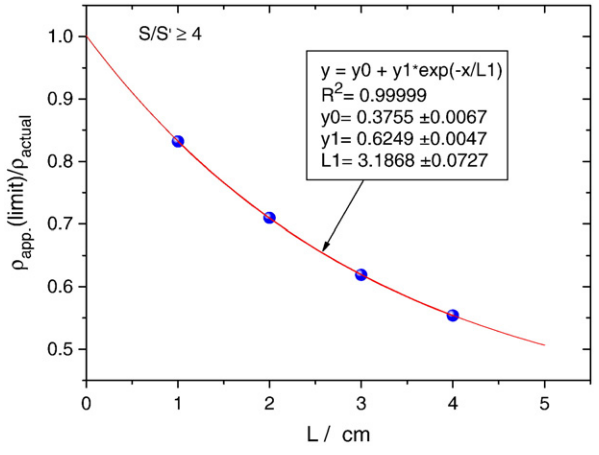

Fig. 11. Variation of the limit apparent resistivity (data for $S/S' = 4$ in Fig. 8) with the thickness of the sample. The solid line corresponds to fitting of data to a first order exponential decay function. The fitting parameters are given in the insert legend.

thickness of the sample. In Fig. 11 those limit values are represented against L. It can be seen that the apparent resistivity decreases exponentially with the thickness of the sample according to Eq. (3).

$$\frac{\rho_{\text{app.limit}}}{\rho_{\text{actual}}} = 0.3755 + 0.6249 \cdot e^{-L/3.1868} \quad (3)$$

Eq. (3) is of major practical importance because it allows to obtain concrete resistivity free of the error inherent to the difference between S and S' when $S \cong S'$. The experimental procedure is simple: experiments have to be performed with a cell so that $S/S' \geq 4$, i.e. for a circular shape sample $\phi_S \geq 2\phi_{S'}$, where ϕ_S and $\phi_{S'}$ are the diameters of S and S', respectively. Then, from the measurement of $\rho_{\text{app.}}$ Eq. (3) allows the direct determination of ρ_{actual}.

Eq. (3) is applicable for the migration experiments. In the case of pure diffusion experiments, the apparent diffusion coefficient is also expected to be dependent on the cell geometry, but not necessarily in the same way as described in Eq. (3).

4. Conclusions

Resistivity measurements performed on cement paste and mortar permeation cells show that the apparent resistivity determined from impedance measurement is highly dependent on the S/S' ratio (cross section of the diaphragm to cross section of the electrolyte). The apparent resistivity decreases exponentially for S/S' values close to one and tends to an asymptotic value as the ratio S/S' increases. That asymptotic value is a function of the thickness of the diaphragm.

FEM numerical simulations show that the experimental observations can be explained in terms of the current dispersion inside the sample. A rule for the design of migration experiments in porous materials like concrete was derived where the resistivity of the sample is readily obtained from the apparent resistivity measured in a configuration where the diameter of the cross section of the diaphragm is at least twice that of the cross section of the electrolyte (Eq. (3)).

Acknowledgments

The authors are grateful to the Spanish “Ministerio de Educación y Ciencia” for financial support under the project BIA2007-66491-C02-01.

References

[1] H.F.W. Taylor, Cement Chemistry, 2nd ed., Thomas Telford, 1997, p. 259.
[2] K.D. Stanish, R.D. Hooton, M.D.A. Thomas, Testing the Chloride Penetration Resistance of Concrete: A Literature Review, Publication No. FHWA-RD-00-142, Federal Highway Administration, USA, 2000.
[3] O. Truc, J.P. Ollivier, M. Carcassès, Cem. Concr. Res. 30 (2000) 217–226.
[4] W. Prince, R. Gagné, Cem. Concr. Res. 31 (2001) 775–780.
[5] M. Castellote, C. Andrade, C. Alonso, Cem. Concr. Res. 31 (2001) 1141–1420.
[6] E. Barsoukov, J.R. Macdonald, Impedance Spectroscopy, 2nd ed., J. Wiley & Sons, 2005, p. 187.
[7] J.L. Tallon, W.H. Robinson, S.I. Smedley, J. Phys. C Solid State Phys. 10 (1977) L579–L583.
[8] M. Prokesch, C. Szeles, J. App. Phys. 100 (2006) 014503.
[9] J. Öijerholm, J. Pan, C. Leygraf, Corros. Sci. 48 (2006) 243–257.
[10] M. Becchi, L. Callegaro, F. Durbiano, V. D'Elia, A. Strigazzi, Rev. Sci. Instrum. 78 (2007) 113902.
[11] W.J. McCarter, R. Brousseau, Cem. Concr. Res. 20 (1990) 981.
[12] B.J. Christensen, T.O. Mason, H.M. Jennings, J. Am. Ceram. Soc. 75 (1992) 939.
[13] Z. Xu, O. Gu, P. Xie, J.J. Beaudoin, Cem. Concr. Res. 23 (1993) 853.
[14] P. Gu, P. Xie, Y. Fu, J.J. Beaudoin, Cem. Concr. Res. 24 (1994) 86.
[15] R.T. Coverdale, B.J. Christensen, R.A. Olson, T.O. Mason, H.M. Jennings, E.J. Garboczi, J. Mater. Sci. 29 (1994) 4984.
[16] B.J. Christensen, R.T. Coverdale, R.A. Olson, S.J. Ford, E.J. Garboczi, H.M. Jennings, T. O. Mason, J. Am. Ceram. Soc. 77 (1994) 2789.
[17] R.T. Coverdale, B.J. Christensen, H.M. Jennings, D.P. Bentz, E.J. Garboczi, J. Mater. Sci. 30 (1995) 712.
[18] M. Keddam, H. Takenouti, X.R. Nóvoa, C. Andrade, C. Alonso, Cem. Concr. Res. 27 (1997) 1191.
[19] M. Cabeza, P. Merino, A. Miranda, X.R. Nóvoa, I. Sánchez, Cem. Concr. Res. 32 (2002) 881.
[20] M. Cabeza, P. Merino, X.R. Nóvoa, I. Sánchez, Cem. Concr. Composites 25 (2003) 351.
[21] C. Andrade, V.M. Blanco, A. Collazo, M. Keddam, X.R. Nóvoa, H. Takenouti, Electrochim. Acta 44 (1999) 4313.
[22] N.E. Hager III, R.C. Domszy, J. Appl. Phys. 96 (2004) 5117.
[23] J.M. Loche, A. Ammar, P. Dumargue, Cem. Concr. Res. 35 (2005) 1797.
[24] A. Aït-Mokhtar, O. Poupard, P. Dumargue, J. Mater. Sci. 41 (2006) 6006.
[25] D.A. Koleva, K. Van Breugel, J.H.W. De Wit, E. Van Westing, N. Boshkov, A.L.A. Fraaij, J. Electrochem. Soc. 154 (2007) E45.
[26] B. Díaz, L. Freire, P. Merino, X.R. Nóvoa, M.C. Pérez, Electrochim. Acta 53 (2008) 7549–7555.
[27] ASTM Standard C 1202-07, Standard Test Method for Electrical Indication of Concrete's Ability to Resist Chloride Ion Penetration. ASTM, http://www.astm.org/, 2007.
[28] B. Díaz, X.R. Nóvoa, M.C. Pérez, Cem. Concr. Comp. 28 (2006) 237–245.